Occurrence, characterisation and fate of Ti and Ag in two Norwegian wastewater treatment plants

Fabio Polesel[1†*], Julia Farkas[2†], Marianne Kjos[3], Patricia Almeida Carvalho[3], Xavier Flores-Alsina[4], Krist V. Gernaey[4], Steffen Foss Hansen[1], Benedek Gy. Plósz[1,5], Andy M. Booth[2*]

[1]DTU Environment, Technical University of Denmark, Bygningstorvet, Building 115, 2800 Kongens Lyngby, Denmark

[2]SINTEF Ocean, Brattørkaia 17C, 7010 Trondheim, Norway

[3]SINTEF Materials and Chemistry, Postboks 4760 Torgarden, 7465 Trondheim, Norway

[4]Process and Systems Engineering Center (PROSYS), Department of Chemical and Biochemical Engineering, Technical University of Denmark, Søltofts Plads, Building 229, 2800 Kongens Lyngby, Denmark

[5]Department of Chemical Engineering, University of Bath, Claverton Down, Bath BA2 7AY, UK

[†]The authors equally contributed to the study.

*Corresponding authors: andy.booth@sintef.no; fabp@env.dtu.dk

Abstract

Due to their widespread application in consumer products, elemental titanium (e.g., titanium dioxide, TiO_2) and silver (Ag), also in nanoparticulate form, are increasingly released from households and industrial facilities to urban wastewater treatment plants (WWTPs). A seven-day sampling campaign was conducted in two full-scale WWTPs in Trondheim (Norway) employing only primary treatment. We assessed the occurrence and elimination of Ti and Ag, and conducted size-based fractionation using sequential filtration of influent samples to separate particulate, colloidal and dissolved fractions. Eight-hour composite influent samples were collected to assess diurnal variations in total Ti and Ag influx. Measured influent Ti concentrations (up to 290 µg L^{-1}) were significantly higher than Ag (<0.15–2.1 µg L^{-1}), being mostly associated with suspended solids (>0.7 µm). Removal efficiencies ≥70% were observed for both elements, requiring for one WWTP to account for the high Ti content (~2 g L^{-1}) in the flocculant. Nano- and micron-sized Ti particles were observed with scanning transmission electron microscopy (STEM) in influent, effluent and biosolids, while Ag nanoparticles were detected in biosolids only. Diurnal profiles of influent Ti were correlated to flow and pollutant concentration patterns (especially total suspended solids), with peaks during the morning and/or evening and minima at night, indicating household discharges as predominant source. Irregular profiles were exhibited by influent Ag, with periodic concentration spikes suggesting short-term discharges from one or few point sources (e.g., industry). Influent Ti and Ag dynamics were reproduced using a disturbance scenario generator model, and we estimated per capita loads of Ti (42–45 mg cap^{-1} d^{-1}) and Ag (0.11 mg cap^{-1} d^{-1}) from households as well as additional Ag load (14–22 g d^{-1}) from point discharge. This is the first study to experimentally and mathematically describe short-term release dynamics and dry-weather sources of emissions of Ti and Ag in municipal WWTPs and receiving environments.

Keywords: nanoparticles, titanium dioxide, silver, wastewater, diurnal variation, modelling

1. Introduction

The release of metals to sewer systems and wastewater treatment plants (WWTPs) has been traditionally linked to industrial discharges (Shafer et al. 1998). Stormwater runoff (containing metals originating from traffic, atmospheric deposition and catchment surfaces) can also contribute to such emissions under wet weather conditions (Becouze-Lareure et al. 2016, Sabin et al. 2005). In the past decade, increasing dry weather discharges from households have been associated with the presence of metals in consumer products, also in the form of pigment-sized particles and metallic nanoparticles (NPs). Titanium (Ti) and silver (Ag) NPs have frequently been detected in WWTP influents (Kiser et al. 2009, Li et al. 2013), owing to their widespread application in clothing (Benn and Westerhoff 2008, Mitrano et al. 2016), washing equipment (Farkas et al. 2011), personal care and hygiene products (Benn and Westerhoff 2008, Contado and Pagnoni 2008, Mackevica et al. 2017, Weir et al. 2012) and food (Weir et al. 2012, Peters et al. 2014).

Attempts have been made to characterize metal fractions in wastewater through size-based fractionation (Kiser et al. 2009, Johnson et al. 2014). Although these studies only assessed either Ti or Ag, they describe a relevant approach for the quantification of metal fractions in particulate, colloidal and dissolved forms. Electron microscopy has proven reliable for identification of Ti and Ag NPs within the different fractions (Kiser et al. 2009, Kaegi et al. 2013). High removal efficiencies (>90%) have been reported in pilot- and full-scale WWTPs for (nano)metallic Ti and Ag (Shafer et al. 1998, Kiser et al. 2009, Li et al. 2013, Johnson et al. 2014, Kaegi et al. 2011, Östman et al. 2017, Westerhoff et al. 2011). This results from sorption to solids and incorporation in primary and secondary sludge, with potential discharge of (nano)metals to soils following agricultural reuse of biosolids as fertilizer. While these

70 studies have investigated the fate and removal in WWTPs with biological treatment, limited
71 information exists for facilities employing only preliminary and primary physico-chemical
72 treatment. These facilities are the most common in Norway, and are known to exhibit reduced
73 removal of conventional pollutants (e.g. solids, organic matter, nutrients) and organic
74 micropollutants (Vogelsang et al. 2006).
75
76 Temporal trends in the dry weather occurrence of Ti and Ag in WWTP influents (diurnal,
77 intra-day, seasonal variations) are largely unknown, likely depending on the type and
78 characteristics of the served catchment. Composite sampling in influents at higher than daily
79 resolution (2-h to 8-h composites) has been previously used to study diurnal release patterns of
80 pharmaceuticals (Plósz et al. 2010) and illicit drugs (Ramin 2016) and to identify point sources
81 of biocide emissions (Bollmann et al. 2014). In situations where removal is incomplete,
82 influent pollutant loads can quickly propagate to effluents, especially in WWTPs with short
83 residence times. Elucidating temporal trends of Ti and Ag in influents can be beneficial for (i)
84 identifying their predominant uses and sources of discharge; (ii) forecasting emission
85 dynamics from WWTPs; and (iii) developing pollutant attenuation strategies by WWTP
86 operators. In this context, influent generator algorithms (Ort et al. 2005; De Keyser et al.,
87 2010; Gernaey et al. 2011) offer a useful tool to extrapolate short-to-medium-term (diurnal to
88 seasonal) dynamics, complementing existing mass flux analysis tools relying (especially for
89 manufactured NPs) on steady-state (Gottschalk et al. 2009) or dynamic predictions at multi-
90 year scale (Sun et al. 2016).
91
92 The objective of the current study was to assess the occurrence and fate of Ti and Ag in two
93 Norwegian WWTPs employing primary sewage treatment. We have (i) evaluated diurnal and

94 intra-day variations in Ti and Ag loads; (ii) developed and tested a method to characterize Ti
95 and Ag as particulate (i.e. associated to suspended solids), colloidal and dissolved fractions;
96 and (iii) identified the presence and the size of Ti and Ag NPs by electron microscopy. In
97 addition, an influent disturbance scenario generator has been adapted to the two WWTP
98 catchments under study, and used to predict occurrence dynamics of influent Ti and Ag and to
99 estimate per capita loads and loads from point sources, based on measured time series. Finally,
100 the fate of Ti and Ag in the two WWTPs was assessed by measuring residual Ti and Ag in final
101 effluents and treated sludge, allowing for the quantification of removal efficiencies during
102 primary wastewater treatment and release to receiving environments.
103
104
105 **2. Materials and methods**
106 ***2.1. Wastewater treatment plants***
107 The city of Trondheim, Norway is served by two main WWTPs (Fig. 1a). Ladehammeren
108 (LARA) and Høvringen (HØRA) have a design capacity of 120,000 PE and 170,000 PE,
109 respectively, with substantial industrial loading contributions (up to 40% for LARA). The
110 wastewater treatment train in LARA and HØRA (Fig. 1b) includes fine screening, sand and fat
111 removal, chemically-aided flocculation-coagulation ($ClFeO_4S$ and polyamine in LARA,
112 polyacrylamide in HØRA) and primary sedimentation (with longitudinal-flow basins in LARA
113 and vertical-flow basins in HØRA). The effluents from each WWTP are discharged into
114 Trondheimsfjord at depths between 40 and 65 m. In both WWTPs, primary sludge is thickened
115 and pasteurized before anaerobic digestion (mesophilic, residence time=15 d), with eventual
116 dewatering through centrifugation (Fig. 1b).
117 **< Figure 1 >**

2.2. Sampling

A seven-day sampling campaign (October 2016) was conducted in parallel in the two WWTPs during a dry weather period. Samples were collected on 6–8th October (Thursday to Saturday) and 10–15th October (Monday to Saturday; for details see Table S1). To determine the total influx and removal efficiencies of Ti and Ag, 24-h composite samples of untreated influent, final effluent and sludge samples were collected (Fig. 1b). Furthermore, 8-h flow-proportional samples of raw influent wastewater were collected to identify potential diurnal influx patterns of Ti and Ag, as well as conventional pollutants. To avoid sample contamination, sampling containers and equipment used for sample treatment and storage (except for metal free centrifuge tubes) were subjected to a multiple step cleaning procedure before each use: surfactant wash, rinse with distilled water, soak in ultrapure HNO_3 (10%) for at least 3 h and rinse with distilled water.

2.2.1. Influx and removal efficiency of Ti and Ag

To determine the incoming loads and the removal efficiency of Ti and Ag in the WWTPs, daily composite samples (LARA: n=6; HØRA: n=5) were collected. The 24-h volume-proportional (ΔV=152 m^3 in LARA, 264 m^3 in HØRA) composite samples of the untreated influent (LARA-IN) and the final effluent (LARA-OUT, HØRA-OUT) were collected using refrigerated automatic samplers. Due to limitations in sampling logistics, 24-h flow-proportional composite samples for HØRA-IN were derived by compositing 8-h flow-proportional samples (see 2.2.2). To account for the hydraulic residence time in the two WWTPs, effluent sample collection was conducted with a delay relative to the influent sampling. Grab samples of biosolids (LARA:

141 *n*=3; HØRA: *n*=2) were collected at the end of the sludge treatment line (Fig. 1b). Biosolids
142 samples were stored at -20°C until analysis.
143
144 *2.2.2. Diurnal influx patterns of Ti and Ag and conventional pollutants*
145 To determine influx patterns and diurnal loading variations of Ti, Ag and conventional
146 pollutants (organic matter, suspended solids, nitrogen, phosphorus) in the WWTP influents,
147 intra-day monitoring was conducted. One-hour time-proportional composite samples
148 (frequency=5 min) were collected each day in clean polyethylene bottles (stored with ice and
149 cooling elements) using portable automatic samplers (Teledyne ISCO®, Lincoln NE, US). At
150 the end of the 24-h interval, 1-h samples were collected and immediately combined flow-
151 proportionally into 8-h samples. Flow-proportional compositing was based on real-time
152 influent flow data collected from the two WWTPs, comparable to previous studies (Plósz et al.
153 2010, Lai et al. 2013, Ramin 2016). The 8-h intervals were selected to cover morning (M),
154 evening (E) and night (N) discharges, based on preliminary assessment of typical flow pattern
155 data and considerations on the catchment size. Samples were processed within 1 h of
156 compositing.
157
158 ***2.3. Sample preparation and analytical methods***
159 *2.3.1. Sample concentration*
160 To achieve quantifiable concentrations of Ti and Ag in IN and OUT 24-h composite samples,
161 40 mL of each sample was concentrated by evaporation immediately after collection. The
162 samples were evaporated to dryness in cleaned glass vials in a water bath (90–95°C) and stored
163 at 4°C prior to analysis by inductively coupled plasma mass spectrometry (ICP-MS). To

164 determine potential background contamination, 40 mL of Milli-Q water (Merck Millipore,
165 USA) (n=3) was evaporated simultaneously with the wastewater samples.
166
167 *2.3.2. Size-based fractionation of Ti and Ag in raw WWTP influent*
168 To determine the occurrence of Ti and Ag in different fractions in the untreated influent
169 wastewater, a size-based fractionation of the pooled 8 h samples (M, E, N) was performed as
170 described in Fig. 2. A detailed description of the approach is provided in the Supporting
171 Information. Briefly, samples (85–100 mL) were sequentially filtered through 2.7 µm and 0.7
172 µm pore size glass fibre filters. The dissolved (ionic) fraction was isolated from the colloidal
173 fraction (0.7 µm filtrate) using ultrafiltration (3 kDa). Ti and Ag were quantified for the 2.7
174 and 0.7 µm filters (particulate fraction), the 0.7 µm filtrate (colloidal and dissolved fraction)
175 and 3 kDa filtrate (dissolved fraction) by ICP-MS (Fig. 2). Total amounts of Ti and Ag in each
176 8-h composite sample were calculated as the sum of the three fractions.
177 **< Figure 2 >**
178
179 *2.3.3. Conventional pollutants analysis*
180 Influent samples (8-h composites) were analysed for conventional pollutants, including total
181 chemical oxygen demand (COD_{tot}), soluble COD (COD_{sol}), total nitrogen (N_{tot}), ammonium
182 nitrogen (NH_4-N), total phosphorus (P_{tot}) and TSS. Dissolved analytes were quantified in the
183 0.7 µm filtrate. Non-filtered and filtered samples were stored in plastic vials and frozen until
184 analysis. COD_{tot}, COD_{sol}, N_{tot} and P_{tot} concentrations were quantified using Hach-Lange®
185 colorimetric kits (LCK314, LCK514, LCK338 and LCK348) and a Hach-Lange® DR 2800
186 spectrophotometer. NH4-N concentrations were quantified using Merck® colorimetric kits

187 (100683) and Merck® Spectroquant® spectrophotometer. Total suspended solids (TSS) were
188 quantified by combining the solid content from the 2.7 µm and 0.7 µm filters.
189
190
191 *2.3.4. Ti and Ag quantification*
192 Ti and Ag were quantified in 24–h composite samples (IN and OUT), biosolids, and in each
193 size fraction of the 8-h influent samples using ICP-MS. Samples of the inorganic flocculant
194 ($ClFeO_4S$) were also analysed for Ti content. For Ag analysis, filters were digested with 8 mL
195 (2.7 µm) or 5 mL (0.7 µm) of 65% HNO_3 in an ultrasonic bath (80°C, 2 h), centrifuged and
196 diluted with ultrapure water (MilliQ). The remaining solution was then supplemented with 8
197 mL (2.7 µm) or 5 mL (0.7 µm) ultrapure water and 1 mL 47–51% hydrofluoric acid (HF),
198 digested for 2 h, centrifuged and diluted with MilliQ water prior to Ti analysis. The 0.7 µm
199 filtrate was diluted (1:1) with 10% HNO_3 and analysed for both Ti and Ag. The 3 kDa filtrate
200 was analysed for Ti and Ag without pre-treatment.
201
202 Evaporated samples were dissolved in 5% HNO_3 overnight. Subsequently, 5 mL of
203 concentrated HNO_3 were added and the samples digested in an ultrasonic bath for 2 h at 80°C.
204 Aliquots were collected for Ag quantification, centrifuged and diluted prior to analysis. For Ti
205 quantification, 2 mL of the digested solution was treated with 200 µL HF, digested for 2 h,
206 diluted and analyzed. Biosolids samples were first digested with HNO_3 in an ultrasonic bath
207 (80°C, 2 h) before HF was added and additional digestion (2 h) was carried out. Samples were
208 analyzed with inductively coupled plasma triple quadrupole mass spectrometry (ICPQQQ,
209 Agilent 8800; Agilent Technologies, USA) equipped with a SPS4 autosampler. Samples were
210 quantified using internal standards ^{115}In and ^{89}Y (Inorganic Ventures, USA).

211

212 *2.3.5. Electron microscopy*

213 Scanning transmission electron microscopy (STEM) coupled with energy-dispersive X-ray
214 spectroscopy (EDS) was used to (i) identify Ti and Ag potentially present as nano-particulates
215 in the total samples and size fractions of wastewater influent, (ii) to characterise Ti and Ag
216 particles (size and shape) and (iii) to study their association with other particulate matter. A
217 detailed summary of the sample preparation procedures is presented in the SI. Briefly,
218 unfiltered and filtered samples (~10 µL) were applied onto TEM grids (copper grids with a
219 lacey carbon film, mesh size 200; Agar Scientific, UK). STEM imaging was performed using
220 an FEI Titan G2 60-300 microscope equipped with a DCOR probe Cs-aberration corrector
221 operating at 300 kV. EDS was conducted with a Bruker SUPERX detector coupled to the same
222 instrument.

223

224 ***2.4 Statistical analysis***

225 Comparative data analyses of Ti and Ag influent concentrations were performed with
226 GraphPad Prism 7 (GraphPad Software Inc., USA). The data sets were analysed for normality
227 (Shapiro-Wilk normality test). To detect significant differences between treatments, data were
228 analysed either with ANOVA followed by Tukey's multiple comparisons test or with the non-
229 parametric Kruskal-Wallis statistics followed by Dunn's test, with significance levels set for
230 $p<0.05$. Correlations between 8-h influent concentrations of Ti, Ag and of conventional
231 pollutants (COD_{tot}, COD_{sol}, N_{tot}, NH_4-N and P_{tot}) were determined using SigmaPlot 11.0
232 (Systat Inc., Germany) to explore possible diurnal co-occurrence patterns.

233

2.5 Modelling dynamics of influent flow rate and concentrations of traditional pollutants, Ti and Ag

Based on 8-h measurements during the sampling campaign, dynamics in the occurrence of Ti and Ag were simulated using a phenomenological influent disturbance scenario generator (Gernaey et al., 2011). This modelling algorithm allows for the generation of high-frequency time series of flow rate and pollutant concentrations in a WWTP influent based on (i) the characteristics (e.g. population, area) of the upstream catchment; and (ii) (dynamic) flow and pollutant load contribution from households, industries, groundwater infiltration and (if relevant) rainfall. A description of the model is provided in the Supporting Information. As compared to previous studies (Snip et al. 2016, Flores-Alsina et al. 2014), a simplified step-by-step calibration procedure was used to fit simulated time series to monitoring results, and to generate consistent concentration profiles for Ti and Ag:

(i) Flow rate predictions were calibrated to high-frequency (5 min for LARA, 2 min for HØRA) measurements using existing knowledge (residential population: 60,000 and 120,000 inhabitants in LARA and HØRA catchments, respectively; groundwater infiltration) and by manually adjusting the flow rate per capita (Q_{PE}, L cap^{-1} d^{-1}), the average industrial flow rate (Q_{ind}, m^3 d^{-1}) and the sewer length (parameter *subarea*).

(ii) Conventional pollutant concentration profiles (8-h samples) were calibrated by manually adjusting household per capita load (g cap^{-1} d^{-1}), based on typical values, and load contributions from industries, in agreement with the type of industries operating in the catchments. In both flow rate (i) and traditional pollutants (ii) model blocks, default diurnal profiles were used. Nevertheless, hourly multiplying factors were adjusted to match intra-day patterns where necessary.

(iii) Correlations between influent concentrations of Ti, Ag and of conventional pollutant indicators (TSS, COD_{tot}, COD_{sol}, N_{tot}, NH_4-N, P_{tot}) were explored. Ti and Ag profiles were generated based on previously established correlations, i.e. using the slope of the correlation as conversion factor, and compared with measured concentration profiles. Per capita loads of Ti and Ag and, if relevant, loads from point sources were estimated.

Correspondence between model simulations and measurements in (i), (ii) and (iii) was verified by considering the coefficient of determination (R^2) and root mean square error (RMSE) as objective functions. Detailed information about the model structure, equations, parameters and stoichiometry are presented in the Supporting Information section.

3. Results

3.1. Occurrence and removal of Ti and Ag

Ti concentrations determined in 24-h composite samples of influent wastewater ranged from 120 µg L^{-1} to 236 µg L^{-1}, and were slightly, but not significantly lower in LARA (154 ± 34 µg L^{-1}) than in HØRA (188 ± 44 µg L^{-1}) (Fig. 3, Table S3). Mean Ti concentrations in the final effluent were 92.8 ± 5.8 µg L^{-1} in LARA and 28.2 ± 4.3 µg L^{-1} in HØRA, while concentrations in biosolids were 1011 ± 59 mg kg^{-1} in LARA and 593 ± 17 mg kg^{-1} in HØRA (Table S3). Removal efficiencies, calculated by comparing influent and effluent Ti concentrations, were 37% ± 13% in LARA and 84% ± 4% in HØRA (Fig. 3). Consistently low removal efficiencies in LARA may be explained by the use of $ClFeO_4S$ as an inorganic flocculant, which was found to contain approximately 1.9 g L^{-1} (1.25 g kg^{-1}) of Ti. When considering the influent Ti load with the flocculant, the removal efficiency in LARA (81%) was in agreement with HØRA (Fig. 3).

Ag concentrations in influent wastewater were approximately three orders of magnitude lower than for Ti. Average Ag concentrations in 24-h composite samples were 0.19 ± 0.02 µg L^{-1} in LARA, while being significantly higher in HØRA (0.59 ± 0.57 µg L^{-1}; $p<0.05$). The large variation of influent Ag concentrations in HØRA was associated with significant intra-day variation, which was also observed in 8-h measurements. These differences were also reflected in effluent concentrations, which were 0.04 ± 0.01 µg L^{-1} in LARA and 0.24 ± 0.37 µg L^{-1} in HØRA. Treated biosolids were found to contain 0.41 ± 0.04 mg kg^{-1} in LARA and 1.10 ± 0.09 mg kg^{-1} in HØRA. Calculated removal efficiencies for Ag were comparable in the two WWTPs, being 78 ± 4% in LARA and 69 ± 16% in HØRA.

< Figure 3 >

3.2. Ti and Ag in WWTP influent

3.2.1. Diurnal variations

The selection of 8-h intervals to assess diurnal variations in Ti and Ag occurrence permitted a comparable and consistent subdivision of the daily influent flow rate at the two WWTPs between morning (M), evening (E) and night (N) discharges. Fractions of daily influent flow rate in M (LARA: 37.5% ± 2.5%; HØRA: 37.6% ± 0.7%), E (LARA: 38.2% ± 1.8%; HØRA: 37.4% ± 0.4%) and N (LARA: 24.3% ± 0.9%; HØRA: 25.0% ± 0.6%) periods accordingly exhibited small intra-day variability and were similar in the two WWTPs, with significantly lower flow in night periods ($p<0.05$).

Figure 4 shows the diurnal profiles of total Ti and Ag concentrations in influents over seven days. Comparable Ti concentrations were quantified in 8-h samples from LARA (66–281 µg L^{-}

305 [1]) and HØRA (92–290 µg L^{-1}), and no significant difference was observed when comparing the
306 two WWTPs for each 8-h interval (Fig. 4a). Ti concentrations followed typical diurnal trends
307 of influent flow rate and pollutant concentrations in municipal WWTP influents (M and/or E
308 peaks, N minima). Accordingly, Ti concentrations in M and E samples were significantly
309 higher than in N samples for both LARA and HØRA ($p<0.05$). Overall, Ti concentrations
310 exhibited rather good correlation ($R^2=0.76$) with TSS in both WWTPs (Fig. 4b). The slope of
311 the correlation was comparable in the two WWTPs, indicating similar amounts of Ti per mg of
312 TSS present in the influent (0.49 µgTi/mgTSS in LARA, 0.47 µgTi/mgTSS in HØRA).
313 Relevant correlations with other conventional pollutant indicators are presented in the
314 Supporting Information. Ti concentrations were found to correlate well with influent COD_{tot}
315 (Fig. S9b, S10b), with $R^2=0.90$ in HØRA.
316
317 Ag concentrations (Fig. 4c) were considerably lower than Ti concentrations in both WWTPs
318 (<0.15–2.1 µg L^{-1}). Ag concentrations at LARA remained relatively constant, whilst an
319 irregular Ag release pattern was observed at HØRA, with considerable variation in E periods.
320 Ag concentrations were significantly higher ($p<0.05$) in E samples from HØRA compared to
321 LARA, whilst HØRA E was significantly higher than HØRA N ($p<0.05$). For LARA, no
322 relevant correlation could be found between influent Ag and conventional pollutant
323 concentrations ($R^2<0.20$). In both Thursday-to-Friday E samples from HØRA, increased Ag
324 concentrations (>1.5 µg L^{-1}, on average four times higher than the other measurements) were
325 detected (Fig. 4c–d, Fig. 9e). In the first sampling day, this was accompanied by a considerable
326 increase of Ag effluent concentrations (Fig. S2). When excluding peak values, Ag
327 concentrations in HØRA exhibited a rather good correlation with P_{tot} ($R^2=0.62$, Fig. 4d). In

328 contrast to Ti, weaker correlations were observed between Ag and TSS or COD_{tot} (Fig. S10d–
329 e).

330 **< Figure 4 >**

331

332 *3.2.2. Fractionation and characterization*

333 The size-based fractionation assessment indicated that most of the influent Ti and Ag occurred
334 in the particulate phase (>0.7 µm), being either in particulate form or associated with
335 wastewater solids (Fig. 5). More than 99% of the influent Ti and >95% of the influent Ag was
336 present in the particulate fraction in both WWTPs (Fig. 5). In LARA, 92% of Ti occurred in
337 the >2.7 µm fraction, with approximately 8% found in the 0.7–2.7 µm fraction. In HØRA, 95%
338 of the Ti was detected in the >2.7 fraction, with ~5% in the 0.7–2.7 µm fraction. These results
339 correlate well with TSS concentrations, for which the 0.7–2.7 µm size fraction represented 8%
340 and 5% of the total concentration in LARA and HØRA, respectively.
341 Approximately 3–5% of Ag occurred in the colloidal and ionic fractions, whilst Ti (≤0.2%)
342 was negligible in these two fractions (Fig. 5). It was not possible to separately quantify
343 colloidal and ionic Ti and Ag, which were therefore combined in the <0.7 µm fraction.

344

345 STEM of influent wastewater samples revealed that elemental Ti and titanium dioxide (TiO_2)
346 were frequently present as particles associated with solids (Fig. 6a–b, Fig. S4). Individual
347 particle diameters ranged from approximately 50 nm to 500 nm, while agglomerates and
348 aggregates reached >500 µm (Fig. 6 b–d; Fig. S3–S4). Furthermore, Ti particles were
349 frequently detected in biosolids, mostly in association with Fe (Fig. 7a). Ti particles were also
350 detected with STEM in effluent samples (Fig. S6), showing their potential release into the
351 receiving environment. Nanoparticulate Ag could not be detected with STEM in influent and

effluent samples, possibly due to low concentrations. However, Ag NPs were detected in treated biosolids samples (Fig. 7b).

< Figure 6 >

< Figure 7 >

3.2.3. Modelling influent Ti and Ag dynamics

The influent flow generator module was calibrated against high-frequency measurements in both HØRA and LARA (Fig. 8a, 9a). A comparably good fit (R^2=0.52–0.79; RMSE=4358–5232 m^3 d^{-1}) was achieved by (i) setting per capita residential discharge (Q_{PE}) to 170 L cap^{-1} d^{-1} in both catchments (LARA: 60,000 inhabitants; HØRA: 120,000 inhabitants), and (ii) adjusting the parameter *subarea* (4 for LARA, 8 for HØRA), which determines the in-sewer residence time and dispersion, in agreement with the surface area of the two catchments (Fig. 1). For HØRA, higher contribution of infiltration (+43%) had to be assumed in the first two days of the sampling campaign due to rainfall in the previous days, resulting in increased flow rate (Fig. 9a) and simultaneous dilution of all influent pollutant concentrations (Fig. S8).

Given that TSS and P_{tot} exhibited the best correlation with Ti and Ag (R^2=0.62–0.76), respectively, concentration profiles of these traditional pollutant indicators were first calibrated (Fig. 8b, 9b–c). TSS was selected over COD_{tot} as it provided a better indication of Ti occurrence in both WWTPs, and in consideration of the similarity in Ti content per amount of TSS. Simulated TSS patterns (R^2=0.75–0.88; RMSE=42.8–62.5 mg L^{-1}) were obtained with similar per capita loads TSS_{PE} = 86 and 95 gTSS cap^{-1} d^{-1} in LARA and HØRA, respectively. Industrial load contribution was set to 14% in LARA and 30% in HØRA, hence justifying higher influent TSS concentrations in HØRA. These numbers reflect the substantial load

376 contribution of food and beverage industry in LARA. Diurnal release patterns of TSS were
377 adjusted by fitting simulations to 1-h concentration profiles, derived from hourly composite
378 samples (Fig. S11). For HØRA, the simulated P_{tot} pattern (R^2=0.69; RMSE=0.9 mg L^{-1}) was
379 obtained with household load $P_{tot,PE}$ = 1.7 gP cap^{-1} d^{-1}.
380 Ti concentration profiles in both WWTPs were predicted from TSS profiles by using the respective
381 average Ti content in TSS, as given in Figure 4b. Simulated time series (Figures 8c, 9d) were
382 generally in agreement with measured profiles (R^2=0.57–0.62; RMSE=41.4–41.6 µg L^{-1}).
383 Accordingly, per capita loads of Ti from household discharges were estimated to be 42.2 mg cap^{-1}
384 d^{-1} for LARA and 44.6 mg cap^{-1} d^{-1} for HØRA.
385
386 A simulated profile of the background Ag concentration in HØRA influent was obtained from
387 the calibrated P_{tot} profile (dotted line, Fig. 9e). This profile described the occurrence of Ag due
388 to baseline activities in the catchment, corresponding to a per capita discharge of 0.11 mg cap^{-1}
389 d^{-1} in HØRA. As expected, this profile did not adequately capture the systematic increase of
390 Ag concentration registered during the sampling campaign, which was therefore attributed to
391 discharge from a point source (e.g., industry). It is thus proposed that a pulse discharge of Ag
392 occurred on Thursday evenings, with the significant increase of influent Ag concentration
393 corresponding to an additional load of 14–22 g d^{-1} from a single point source.
394 **< Figure 8 >**
395 **< Figure 9 >**
396
397 **4. Discussion**
398 ***4.1. Influx, removal and release of Ti***

399 Ti concentrations in untreated influent determined in this study (154 ± 34 µg L^{-1} in LARA, 188
400 ± 44 µg L^{-1} in HØRA) are in agreement with other studies, which reported mean Ti
401 concentrations of 185–377 µg L^{-1} in WWTP influents in Arizona (Kiser et al. 2009, Westerhoff
402 et al. 2011).
403 Despite employing similar primary treatment (comprising both mechanical and chemical
404 steps), calculated Ti removal in LARA was significantly lower (37 ± 12%) than for HØRA
405 (84% ± 4%). This is due to the application of $ClFeO_4S$ flocculant in LARA, which was found
406 to contain ~2 g L^{-1} Ti. When considering influent Ti loading with untreated wastewater and
407 flocculant, the removal efficiency was estimated to be 81% for LARA, similarly to what
408 observed in HØRA. This further explains the 2-fold increase of Ti concentrations in biosolids
409 in LARA (1010 µg g^{-1}) compared to HØRA (593 µg g^{-1}), despite the lower Ti influent values
410 (Fig. 3). For the first time, this study has shown that inorganic flocculants represent a
411 significant source of Ti in WWTPs. Future studies should therefore consider all the potential
412 influent streams when performing mass balances and calculating removal efficiencies of Ti.
413
414 A comparison with previous investigations revealed that measured Ti removal efficiencies in
415 HØRA (on average 84%) were lower than observations in other WWTPs with secondary and
416 tertiary treatment, where Ti removal efficiencies are typically >90% (Kiser et al. 2009,
417 Westerhoff et al. 2011). HØRA typically achieves TSS removal efficiencies of 75% (data not
418 shown), well below the performance of WWTPs employing secondary treatment. Therefore,
419 incomplete Ti removal in HØRA (when compared to secondary/tertiary WWTPs) can be
420 attributed to the presence of primary treatment only. Furthermore, differences may be
421 attributed to the fact that earlier removal efficiency determinations were made using grab

422 sampling of influent and effluent, i.e. without the use of composite samples (e.g., over 24 h) as
423 in the current investigation.
424
425 Ti removal in HØRA is most likely related to association with solids (Fig. 4–5), which are
426 mostly removed during settling and other separation processes. Ti concentrations in biosolids
427 from LARA and HØRA were comparable to those measured in primary sludge (700 ± 200 µg
428 g^{-1}) from a WWTP in the US (Kiser et al. 2009). Previously reported Ti concentration in
429 sewage sludge and biosolids ranged from 97 to 4510 mg kg^{-1} (Kim et al. 2012, Westerhoff et
430 al. 2015). Furthermore, we observed agglomerates and aggregates of TiO_2 particles reaching
431 500 nm to >1 µm in size (Fig. 6, Fig. S3), which may also settle independently. This is in
432 agreement with previous research reporting a 97% removal of TiO_2 NPs in the presence of
433 biosolids, and a 65% removal in the absence of biosolids caused by aggregation and
434 sedimentation (Wang et al. 2012).
435
436 ***4.2. Influx, removal and release of Ag***
437 Influent Ag concentrations (<150–2140 ng L^{-1}) were 100–1000 times lower than Ti
438 concentrations in both WWTPs, being generally in good agreement with other findings. A
439 recent study in Sweden reported average total Ag concentrations of 10–2200 ng L^{-1} (490 ± 670
440 ng L^{-1}) in the influent of 11 WWTPs (Östman et al. 2017). In a monitoring campaign in several
441 WWTPs in the UK, total Ag concentrations were on average 3310 ng L^{-1}, with approximately
442 12 ng L^{-1} (0.36%) being in the colloidal fraction (there defined with size 2–450 nm) (Johnson
443 et al. 2014). In Germany, total Ag influent concentrations ranged from 350 to 760 ng L^{-1}, with
444 a peak concentration of 3050 ng L^{-1} in one of the WWTPs (Li et al. 2013). Ag in WWTP

influent may also include its sulfidized form, which is known to form during transport in sewers (Kaegi et al., 2013).

The removal efficiency of Ag in the current study was on average 69–78 %, being 10 % higher in LARA than HØRA. Reduced removal efficiency was observed during the first sampling day at HØRA (47%), most likely resulting from the influent Ag concentration peak during Thursday-Friday evening (Fig. 8c; Fig. S2). Due to the relatively short WWTP residence time, this peak propagated to the effluent, resulting in an increased effluent Ag concentration of 0.9 µg L^{-1}. Higher removal efficiencies (>93%) compared to the current study have been reported elsewhere (Li et al. 2012, Johnson et al. 2014, Östman et al. 2017). Similarly to Ti, all the WWTPs investigated employed secondary and/or tertiary treatment, which may have led to increased Ag removal.

4.3. Characterization of Ti and Ag

Characterization of Ti and Ag was performed through size-based fractionation by means of sequential filtration and STEM analyses. Detected Ti was strongly associated with wastewater solids, with >99% of influent concentration being measured in the particulate fraction (>0.7 µm) in both WWTPs. TiO_2 nano- and micro-particles were frequently detected using STEM analysis in both untreated samples and >0.7 µm fraction, with particle size ranging from 50–500 nm up to more than 1 µm. The association of TiO_2 to solids is suggested as the main reason for most Ti being in the particulate fraction, supported by a strong correlation between Ti and TSS for both WWTPs (Fig. 4b). Strong association of Ti with suspended solids is consistent with other studies, where 81–96% of the total Ti in wastewater influent was associated with solids >0.7 µm (Kiser et al. 2009).

469 Most Ag (95–97 %) in wastewater influent was in the particulate fraction (>0.7 μm). However,
470 it was not possible to detect Ag (nano)particles with STEM in influent or effluent samples.
471 This may be due to the low Ag concentrations and the association of both Ag particles and ions
472 to solids, as shown in previous studies (Li et al. 2013, Kaegi et al. 2011, Wang et al. 2012,
473 Kiser et al. 2010). Ag NPs were observed in biosolids (Fig. 7b), but it is unclear whether they
474 were related to the presence of Ag in NP form (at low concentrations) in the influent, or
475 whether Ag in dissolved form underwent transformation (e.g., to Ag_2S NPs) during treatment
476 (Kim et al., 2010). Further investigation should therefore elucidate whether Ag released with
477 WWTP effluents occurs in nanoparticulate form, also in consideration of influent-to-effluent
478 load propagation in Norwegian WWTPs with primary treatment.
479
480 ***4.4. Release patterns and sources of discharge***
481 Diurnal Ti concentrations at both WWTPs were characterized by M and/or E peaks with a
482 significant decrease during the night period. This indicates that Ti discharge follows household
483 discharges, and is in agreement with previous observations for similar catchments and
484 conditions (Becouze-Lareure et al. 2016). Conversely, Ag concentrations in HØRA influent
485 exhibited a significant increase during Thursday-Friday evening periods, resulting from short-
486 term discharge to the sewer system. Ag discharges to HØRA appear to be influenced by one
487 point source, possibly related to industrial activities. Similar observations in WWTP influent
488 have been made for Ti, where industrial contribution to increased Ti loading was postulated
489 (Kiser et al. 2009).
490
491 Correlation analysis was used to elucidate sources of discharge by assessing co-occurrence of
492 Ti and Ag with other parameters routinely measured in untreated wastewater. This

493 methodology has been previously applied to identify sources and pathways of pharmaceutical
494 discharge (Plósz et al. 2010, Snip et al. 2016). The rather strong correlation of Ti with TSS
495 suggests either a strong binding to solids, which may have occurred to some extent during in-
496 sewer transport, or a common source. Interestingly, comparable amounts of Ti were quantified
497 per mass of TSS in both WWTPs (0.47–0.49 μg Ti $mgTSS^{-1}$) over the duration of the sampling
498 campaign, suggesting rather similar binding potential to solids in raw sewage.
499
500 Despite the consistent association with wastewater solids, Ag exhibited a rather good
501 correlation with P (except for recurring peak values). The co-occurrence of Ag and P may
502 therefore suggest their combined discharge in wastewater. Phosphorus (mostly in phosphate
503 form) is present in commercial products such as detergents, despite regulatory efforts to limit
504 its use. Accordingly, a number of studies have reported on the release of Ag from textiles
505 during washing with (Geranio et al. 2009, Lorenz et al. 2012) or without (Mitrano et al. 2014,
506 Lombi et al. 2014) P-containing detergents. Furthermore, silver phosphate was identified in
507 unwashed textiles and its formation was observed after washing with P-containing detergent
508 (Lombi et al. 2014). Ag release was also shown to occur from commercial washing machines
509 (Farkas et al. 2011) during laundry cycles. Considering the permissible phosphate content in
510 dishwasher detergents (as of October 2016) in Norway, another potential source of Ag may be
511 dishwashing. Although food containers have been shown to contain and release Ag in
512 nanoparticulate form (Mackevica et al. 2016), no conclusive evidence exists on the release as a
513 result of dishwashing. Furthermore, phosphate is widely used in commercial toothpaste, while
514 Ag has been quantified in both toothpaste (Benn et al. 2010) and toothbrushes (Mackevica et
515 al. 2017). Observations from the current study suggest release of Ag from consumer products

516 through washing and personal care procedures is the main source of *background* emissions to
517 WWTPs (i.e. without considering temporary industrial discharges).
518
519 The information obtained on diurnal patterns and co-occurrence with wastewater pollutants
520 was used to predict Ti and Ag occurrence profiles in WWTP influents. Whilst influent
521 generator models have been developed and calibrated for conventional pollutants (Flores-
522 Alsina et al. 2014) and organic micropollutants (Snip et al. 2016), this study represents a first
523 application to metals. Per capita discharge of Ti in the two catchments was estimated to be 42–
524 45 mg cap^{-1} d^{-1}, in agreement with previous estimations (Kiser et al. 2009). The estimated Ag
525 load from a point source in HØRA catchment was 14–22 g d^{-1}, up to >70% of total influent
526 load during Thursday evening periods. These estimations are in good agreement with
527 calculated emissions from a single laundry facility in a Swiss WWTP catchment (Kaegi et al.
528 2015). For compounds (such as Ti, Ag and other nano-metals) of relatively unknown usage
529 volumes, detailed knowledge of major sources of discharge and estimation of residential and
530 point source contributions would be highly beneficial for short- and long-term predictions of
531 release dynamics.
532
533 **5. Conclusions**
534 The current study quantified and characterized Ti and Ag in influent, effluent and biosolids of
535 two Norwegian WWTPs (LARA and HØRA), with specific attention towards NPs. Intra-day
536 variations of Ti and Ag influx patterns were assessed, and potential discharge sources were
537 determined.
538 • Mechanical and physico-chemical treatment is sufficient to remove ≥70% of Ti and Ag,
539 mostly through binding to solids and solid-liquid separation processes (e.g., primary

sedimentation). As certain WWTP flocculants contain high concentrations of Ti, it is necessary to account for this additional influx when calculating accurate mass balances.

- Ti was frequently detected as nano- and micronized particles bound to wastewater solids, with total amounts correlating strongly with TSS concentrations. The absence of detectable Ag NPs in influent and effluents may be a result of their low concentrations, although their occurrence can be hypothesized based on detection in biosolids.
- Influent Ti concentrations followed typical flow and pollutant trends, i.e. significant decrease during night, indicating households as major discharge sources. The significant weekly spike in influent Ag concentration observed for HØRA is indicative of a point source industrial discharge. Background influent Ag levels correlated positively with total phosphorus concentrations, suggesting release from textiles and personal care products as primary discharge sources.
- For the first time, an influent generator model was successfully used for prediction of Ti and Ag profiles in WWTP influent. Model simulations allowed short-term release dynamics of Ti and Ag to be described and loads from households and point sources (industries) to be determined, thus complementing existing fate and emission models for (nano)metals. Model-based approaches can further serve as a means to enforce chemical abatement strategies by identifying and reducing point source emissions.

Acknowledgments

This study was supported by the Norwegian Research Council project NanoWASTE (GA: 238972). The authors are particularly grateful to WWTP operators at LARA and HØRA, especially Grete Klippenvåg Støen. Dr Flores-Alsina gratefully acknowledges the financial support of the collaborative international consortium WATERJPI2015 WATINTECH of the

564 Water Challenges for a Changing World Joint Programming Initiative (project ID 196) and the
565 funds provided by the Danish Council for Independent Research under the project
566 GREENLOGIC (project number: 7017-00175B).
567
568
569
570 **References**
571 Becouze-Lareure, C., Dembélé, A., Coquery, M., Cren-Olivé, C., Barillon, B. and Bertrand-
572 Krajewski, J.L. (2016). Source characterisation and loads of metals and pesticides in urban
573 wet weather discharges. Urban Water Journal 13(6), 600-617.
574 Benn, T.M. and Westerhoff, P. (2008) Nanoparticle Silver Released into Water from
575 Commercially Available Sock Fabrics. Environmental Science & Technology 42(11), 4133-
576 4139.
577 Benn, T., Cavanagh, B., Hristovski, K., Posner, J.D. and Westerhoff, P. (2010) The Release of
578 Nanosilver from Consumer Products Used in the Home. Journal of Environmental Quality
579 39(6), 1875-1882.
580 Bollmann, U.E., Tang, C., Eriksson, E., Jönsson, K., Vollertsen, J. and Bester, K. (2014)
581 Biocides in urban wastewater treatment plant influent at dry and wet weather:
582 Concentrations, mass flows and possible sources. Water Research 60(Supplement C), 64-74.
583 Contado, C. and Pagnoni, A. (2008) TiO2 in Commercial Sunscreen Lotion: Flow Field-Flow
584 Fractionation and ICP-AES Together for Size Analysis. Analytical Chemistry 80(19), 7594-
585 7608.

586 De Keyser, W., Gevaert, V., Verdonck, F., De Baets, B., Benedetti, L. (2010). An emission
587 time series generator for pollutant release modelling in urban areas. Environmental
588 Modelling & Software 25(4), 554–561.
589 Farkas, J., Peter, H., Christian, P., Gallego Urrea, J.A., Hassellöv, M., Tuoriniemi, J.,
590 Gustafsson, S., Olsson, E., Hylland, K. and Thomas, K.V. (2011) Characterization of the
591 effluent from a nanosilver producing washing machine. Environment International 37(6),
592 1057-1062.
593 Flores-Alsina, X., Saagi, R., Lindblom, E., Thirsing, C., Thornberg, D., Gernaey, K.V. and
594 Jeppsson, U. (2014) Calibration and validation of a phenomenological influent pollutant
595 disturbance scenario generator using full-scale data. Water Research 51(Supplement C),
596 172-185.
597 Geranio, L., Heuberger, M. and Nowack, B. (2009) The Behavior of Silver Nanotextiles during
598 Washing. Environmental Science & Technology 43(21), 8113-8118.
599 Gernaey, K.V., Flores-Alsina, X., Rosen, C., Benedetti, L. and Jeppsson, U. (2011) Dynamic
600 influent pollutant disturbance scenario generation using a phenomenological modelling
601 approach. Environmental Modelling & Software 26(11), 1255-1267.
602 Gottschalk, F., Sonderer, T., Scholz, R.W. and Nowack, B. (2009) Modeled Environmental
603 Concentrations of Engineered Nanomaterials (TiO2, ZnO, Ag, CNT, Fullerenes) for
604 Different Regions. Environmental Science & Technology 43(24), 9216-9222.
605 Johnson, A.C., Jürgens, M.D., Lawlor, A.J., Cisowska, I. and Williams, R.J. (2014) Particulate
606 and colloidal silver in sewage effluent and sludge discharged from British wastewater
607 treatment plants. Chemosphere 112(Supplement C), 49-55.

608 Kaegi, R., Voegelin, A., Sinnet, B., Zuleeg, S., Hagendorfer, H., Burkhardt, M. and Siegrist,
609 H. (2011) Behavior of Metallic Silver Nanoparticles in a Pilot Wastewater Treatment Plant.
610 Environmental Science & Technology 45(9), 3902-3908.
611 Kaegi, R., Voegelin, A., Ort, C., Sinnet, B., Thalmann, B., Krismer, J., Hagendorfer, H.,
612 Elumelu, M. and Mueller, E. (2013) Fate and transformation of silver nanoparticles in urban
613 wastewater systems. Water Research 47(12), 3866-3877.
614 Kaegi, R., Voegelin, A., Sinnet, B., Zuleeg, S., Siegrist, H. and Burkhardt, M. (2015)
615 Transformation of AgCl nanoparticles in a sewer system — A field study. Science of the
616 Total Environment 535(Supplement C), 20-27.
617 Kim, B., Park, C.S., Murayama, M., Hochella, M.F. (2010) Discovery and characterization of
618 silver sulfide nanoparticles in final sewage sludge products. Environmental Science &
619 Technology 44(19), 7509–7514.
620 Kim, B., Murayama, M., Colman, B.P. and Hochella, M.F. (2012) Characterization and
621 environmental implications of nano- and larger TiO2 particles in sewage sludge, and soils
622 amended with sewage sludge. Journal of Environmental Monitoring 14(4), 1128-1136.
623 Kiser, M.A., Westerhoff, P., Benn, T., Wang, Y., Pérez-Rivera, J. and Hristovski, K. (2009)
624 Titanium Nanomaterial Removal and Release from Wastewater Treatment Plants.
625 Environmental Science & Technology 43(17), 6757-6763.
626 Kiser, M.A., Ryu, H., Jang, H., Hristovski, K. and Westerhoff, P. (2010) Biosorption of
627 nanoparticles to heterotrophic wastewater biomass. Water Research 44(14), 4105-4114.
628 Lai, F.Y., Bruno, R., Leung, H.W., Thai, P.K., Ort, C., Carter, S., Thompson, K., Lam, P.K.S.
629 and Mueller, J.F. (2013) Estimating daily and diurnal variations of illicit drug use in Hong
630 Kong: A pilot study of using wastewater analysis in an Asian metropolitan city. Forensic
631 Science International 233(1), 126-132.

632 Li, L., Hartmann, G., Döblinger, M. and Schuster, M. (2013) Quantification of Nanoscale
633 Silver Particles Removal and Release from Municipal Wastewater Treatment Plants in
634 Germany. Environmental Science & Technology 47(13), 7317-7323.
635 Lombi, E., Donner, E., Scheckel, K.G., Sekine, R., Lorenz, C., Goetz, N.V. and Nowack, B.
636 (2014) Silver speciation and release in commercial antimicrobial textiles as influenced by
637 washing. Chemosphere 111(Supplement C), 352-358.
638 Lorenz, C., Windler, L., von Goetz, N., Lehmann, R.P., Schuppler, M., Hungerbühler, K.,
639 Heuberger, M. and Nowack, B. (2012) Characterization of silver release from commercially
640 available functional (nano)textiles. Chemosphere 89(7), 817-824.
641 Mackevica, A., Olsson, M.E. and Hansen, S.F. (2016) Silver nanoparticle release from
642 commercially available plastic food containers into food simulants. Journal of Nanoparticle
643 Research 18(1), 5.
644 Mackevica, A., Olsson, M.E. and Hansen, S.F. (2017) The release of silver nanoparticles from
645 commercial toothbrushes. Journal of Hazardous Materials 322(Part A), 270-275.
646 Mitrano, D.M., Rimmele, E., Wichser, A., Erni, R., Height, M. and Nowack, B. (2014)
647 Presence of Nanoparticles in Wash Water from Conventional Silver and Nano-silver
648 Textiles. ACS Nano 8(7), 7208-7219.
649 Mitrano, D.M., Lombi, E., Dasilva, Y.A.R. and Nowack, B. (2016) Unraveling the Complexity
650 in the Aging of Nanoenhanced Textiles: A Comprehensive Sequential Study on the Effects
651 of Sunlight and Washing on Silver Nanoparticles. Environmental Science & Technology
652 50(11), 5790-5799.
653 Ort, C., Schaffner, C., Giger, W., Gujer, W. (2005). Modelling stochastic load variations in
654 sewer systems. Water Science & Technology 52(5), 113−122.

655 Peters, R.J.B., van Bemmel, G., Herrera-Rivera, Z., Helsper, H.P.F.G., Marvin, H.J.P., Weigel,
656 S., Tromp, P.C., Oomen, A.G., Rietveld, A.G. and Bouwmeester, H. (2014)
657 Characterization of Titanium Dioxide Nanoparticles in Food Products: Analytical Methods
658 To Define Nanoparticles. Journal of Agricultural and Food Chemistry 62(27), 6285-6293.
659 Plósz, B.G., Leknes, H., Liltved, H. and Thomas, K.V. (2010) Diurnal variations in the
660 occurrence and the fate of hormones and antibiotics in activated sludge wastewater
661 treatment in Oslo, Norway. Science of the Total Environment 408(8), 1915-1924.
662 Ramin, P. (2016) Modelling illicit drug fate in sewers for wastewater-based epidemiology.
663 PhD, Technical University of Denmark.
664 Sabin, L.D., Lim, J.H., Stolzenbach, K.D. and Schiff, K.C. (2005) Contribution of trace metals
665 from atmospheric deposition to stormwater runoff in a small impervious urban catchment.
666 Water Research 39(16), 3929-3937.
667 Shafer, M.M., Overdier, J.T. and Armstong, D.E. (1998). Removal, partitioning, and fate of
668 silver and other metals in wastewater treatment plants and effluent-receiving streams.
669 Environmental Toxicology and Chemistry 17(4), 630-641.
670 Snip, L.J.P., Flores-Alsina, X., Aymerich, I., Rodríguez-Mozaz, S., Barceló, D., Plósz, B.G.,
671 Corominas, L., Rodriguez-Roda, I., Jeppsson, U. and Gernaey, K.V. (2016) Generation of
672 synthetic influent data to perform (micro)pollutant wastewater treatment modelling studies.
673 Science of the Total Environment 569(Supplement C), 278-290.
674 Sun, T.Y., Bornhöft, N.A., Hungerbühler, K. and Nowack, B. (2016) Dynamic Probabilistic
675 Modeling of Environmental Emissions of Engineered Nanomaterials. Environmental
676 Science & Technology 50(9), 4701-4711.

677 Vogelsang, C., Grung, M., Jantsch, T.G., Tollefsen, K.E. and Liltved, H. (2006) Occurrence
678 and removal of selected organic micropollutants at mechanical, chemical and advanced
679 wastewater treatment plants in Norway. Water Research 40(19), 3559-3570.
680 Wang, Y., Westerhoff, P. and Hristovski, K.D. (2012) Fate and biological effects of silver,
681 titanium dioxide, and C60 (fullerene) nanomaterials during simulated wastewater treatment
682 processes. Journal of Hazardous Materials 201–202(0), 16-22.
683 Weir, A., Westerhoff, P., Fabricius, L., Hristovski, K. and von Goetz, N. (2012) Titanium
684 Dioxide Nanoparticles in Food and Personal Care Products. Environmental Science &
685 Technology 46(4), 2242-2250.
686 Westerhoff, P., Song, G., Hristovski, K. and Kiser, M.A. (2011) Occurrence and removal of
687 titanium at full scale wastewater treatment plants: implications for TiO2 nanomaterials.
688 Journal of Environmental Monitoring 13(5), 1195-1203.
689 Westerhoff, P., Lee, S., Yang, Y., Gordon, G.W., Hristovski, K., Halden, R.U. and Herckes, P.
690 (2015) Characterization, Recovery Opportunities, and Valuation of Metals in Municipal
691 Sludges from U.S. Wastewater Treatment Plants Nationwide. Environmental Science &
692 Technology 49(16), 9479-9488.
693 Östman, M., Lindberg, R.H., Fick, J., Björn, E. and Tysklind, M. (2017) Screening of biocides,
694 metals and antibiotics in Swedish sewage sludge and wastewater. Water Research
695 115(Supplement C), 318-328.

696 **Figures**

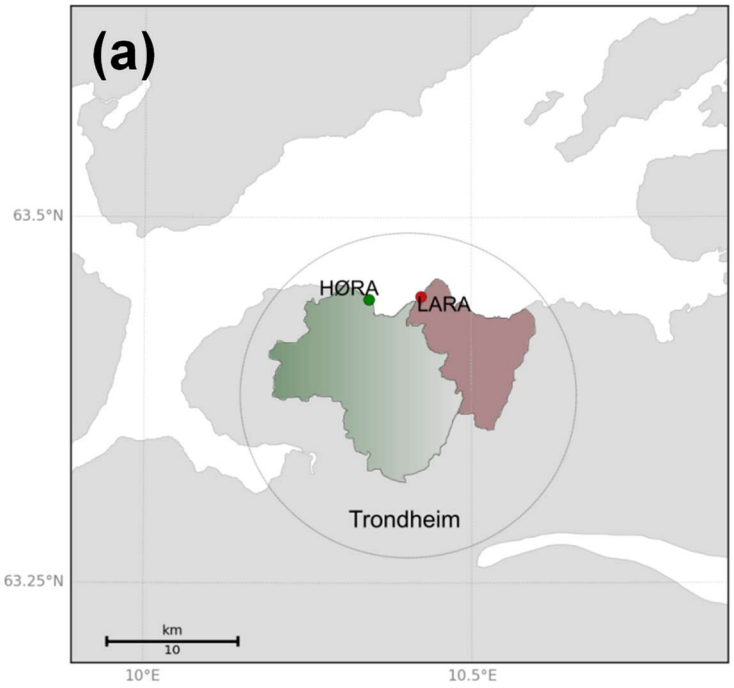

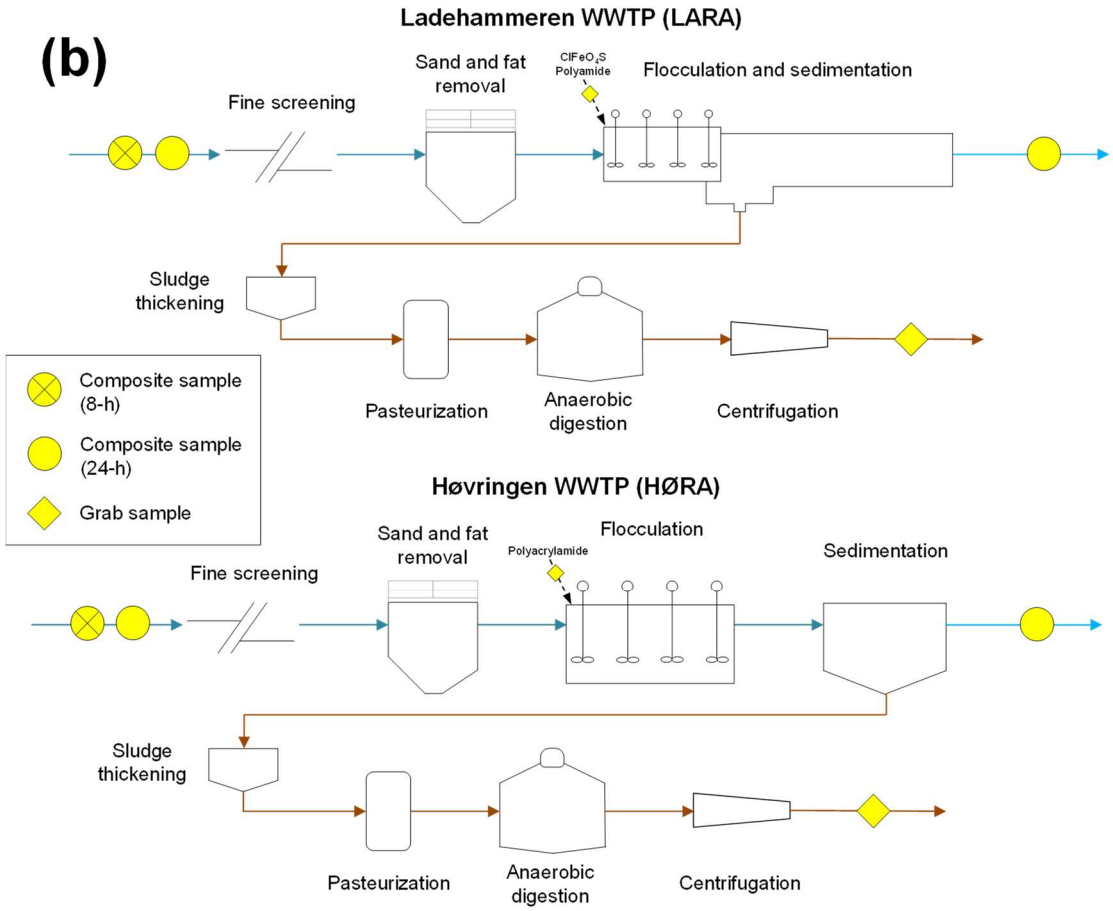

697

Figure 1. (a) Map of Trondheim, with location of LARA and HØRA WWTPs and area of the served catchments (19.3 and 48.3 km^2 respectively). (b) Flow-sheet diagram of LARA and HØRA. Yellow symbols denote the three sampling points and the respective sampling modes, i.e. untreated influent (8-h flow-proportional composite samples, 24-h volume- or flow-proportional samples), final effluent (24-h volume-proportional composite samples) and treated sludge (grab samples).

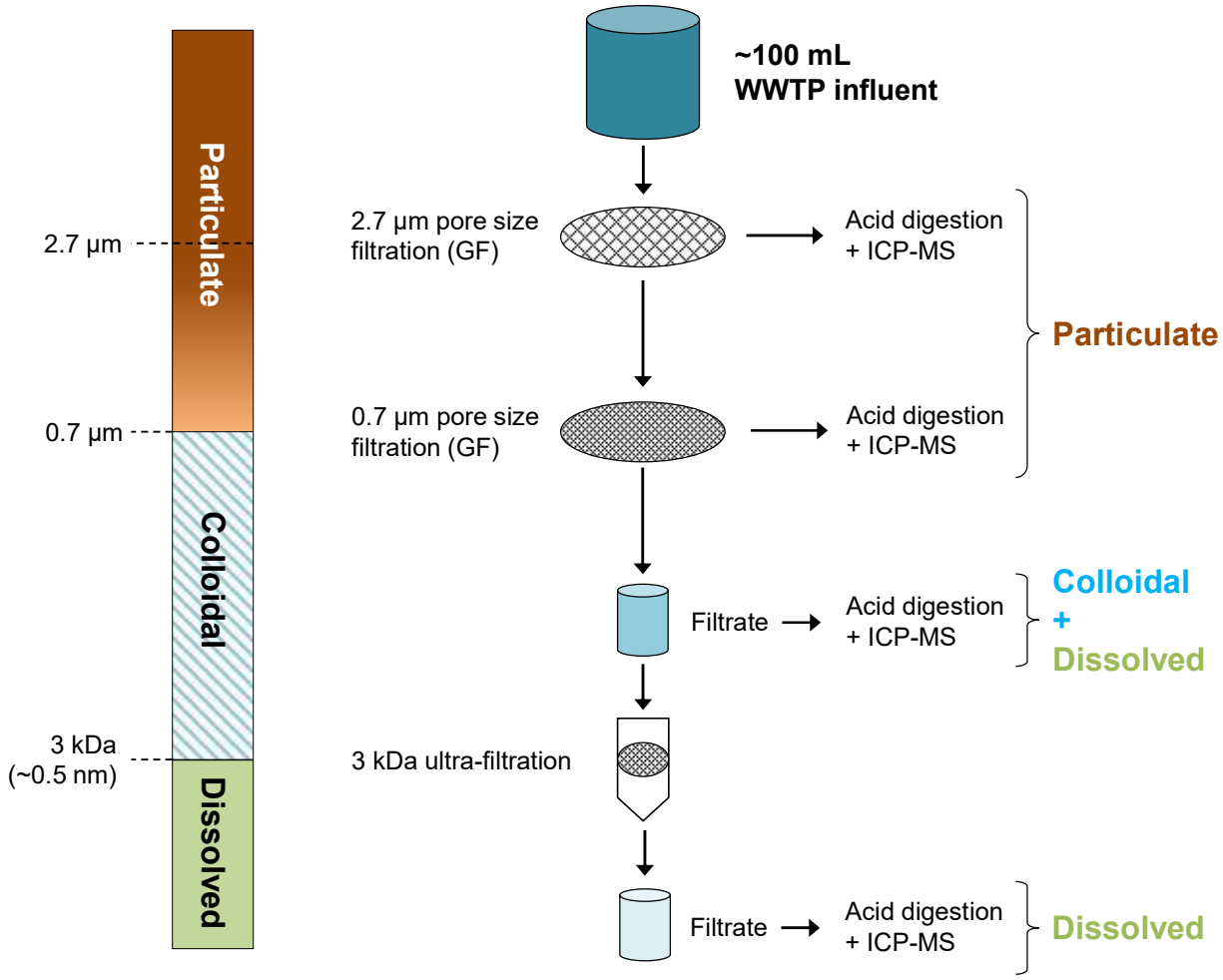

704

705 **Figure 2.** Fractionation procedure used to separate and characterize Ti and Ag as particulate,

706 colloidal and dissolved (ionic) fractions.

707

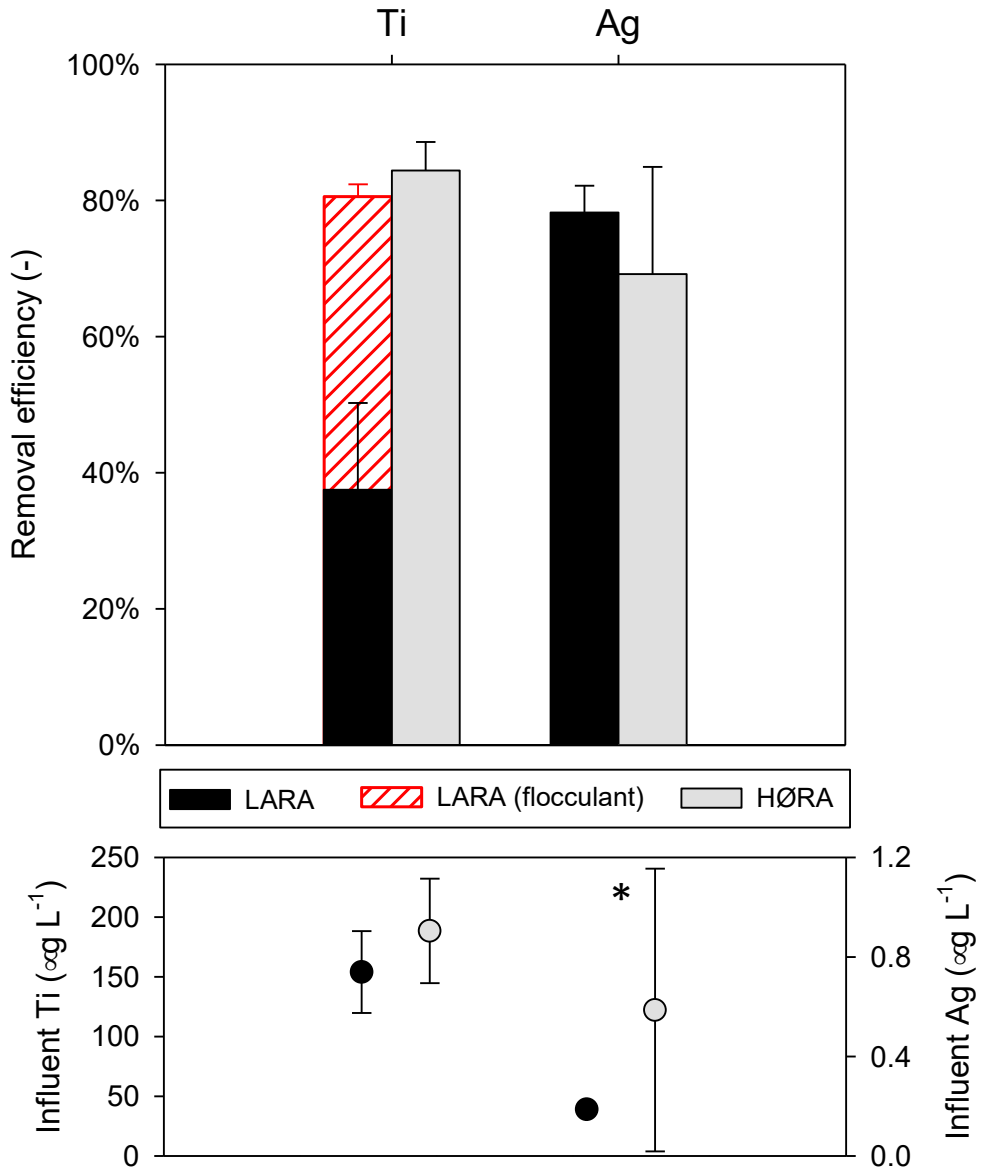

708

709 **Figure 3.** Removal efficiencies and influent concentrations (mean and standard deviation) of
710 Ti and Ag in LARA (*n*=6) and HØRA (*n*=5). For LARA, removal efficiency of Ti was also
711 calculated by accounting for influent Ti load with flocculant. Reported influent Ti and Ag
712 concentrations were measured in 24-h composite influent samples. The asterisk (*) denotes
713 significant differences ($p<0.05$) between the two WWTPs.

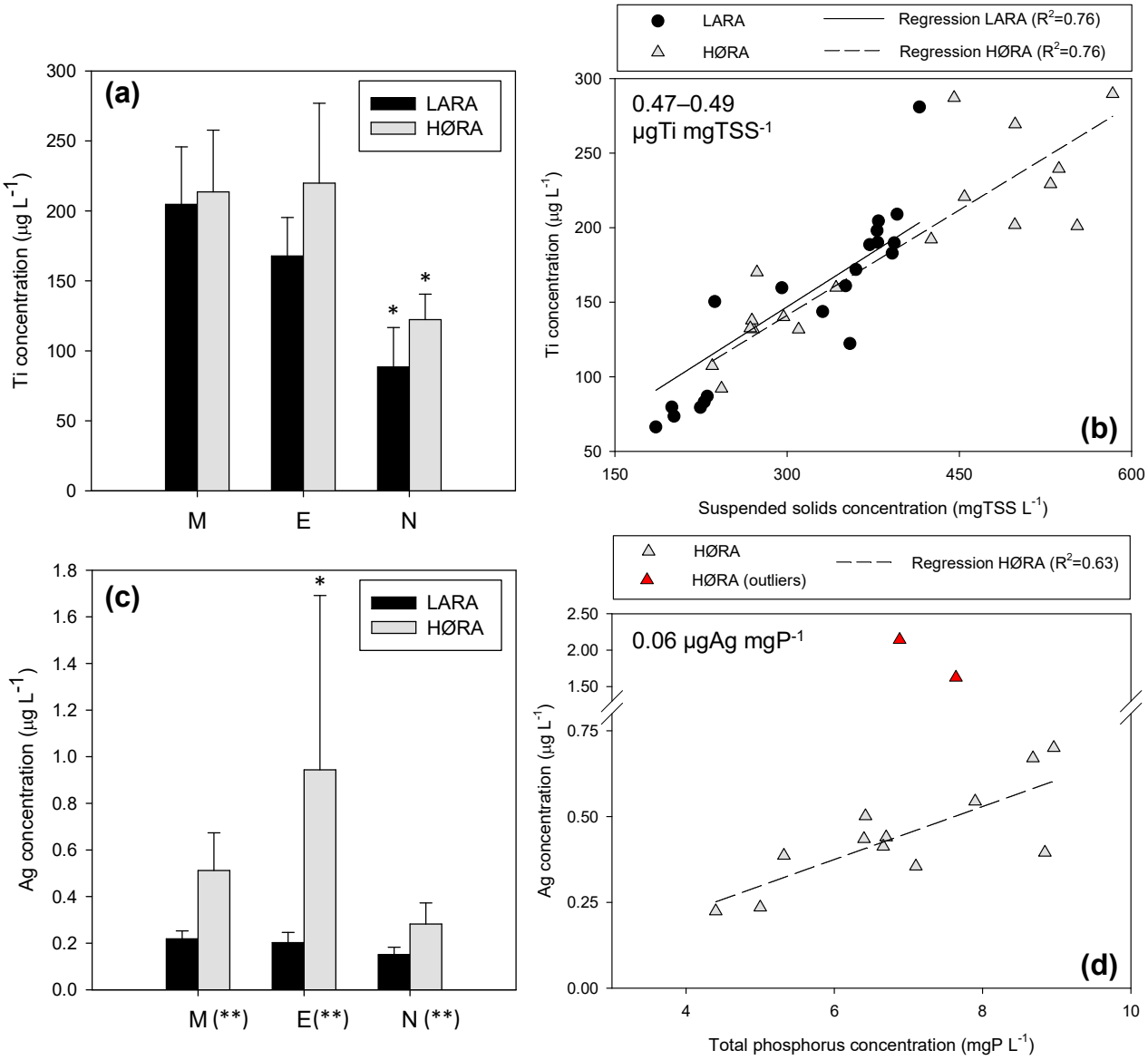

714

715 **Figure 4.** Diurnal variations in the occurrence of total Ti (a–b) and Ag (c–d) in LARA and
716 HØRA WWTP influents during the 7-day sampling campaign. Mean total Ti (a) and Ag (c)
717 concentrations are shown for morning (M), evening (E) and night (N) 8 h intervals.
718 Correlations are shown between influent Ti and TSS concentrations in LARA and HØRA (b)
719 and between influent Ag and total phosphorus concentrations in HØRA (d). For Ag, red
720 symbols denote outliers (concentrations higher than 1.5 µg L^{-1}). Asterisks in (a) and (c) denote
721 significant differences between data sets. One asterisk (*) indicates that, for the same WWTP,
722 the influent concentration in one 8-h period is significantly different from both other 8-h

periods. Two asterisks (**) denote significant differences between the two WWTPs for the same 8-h period.

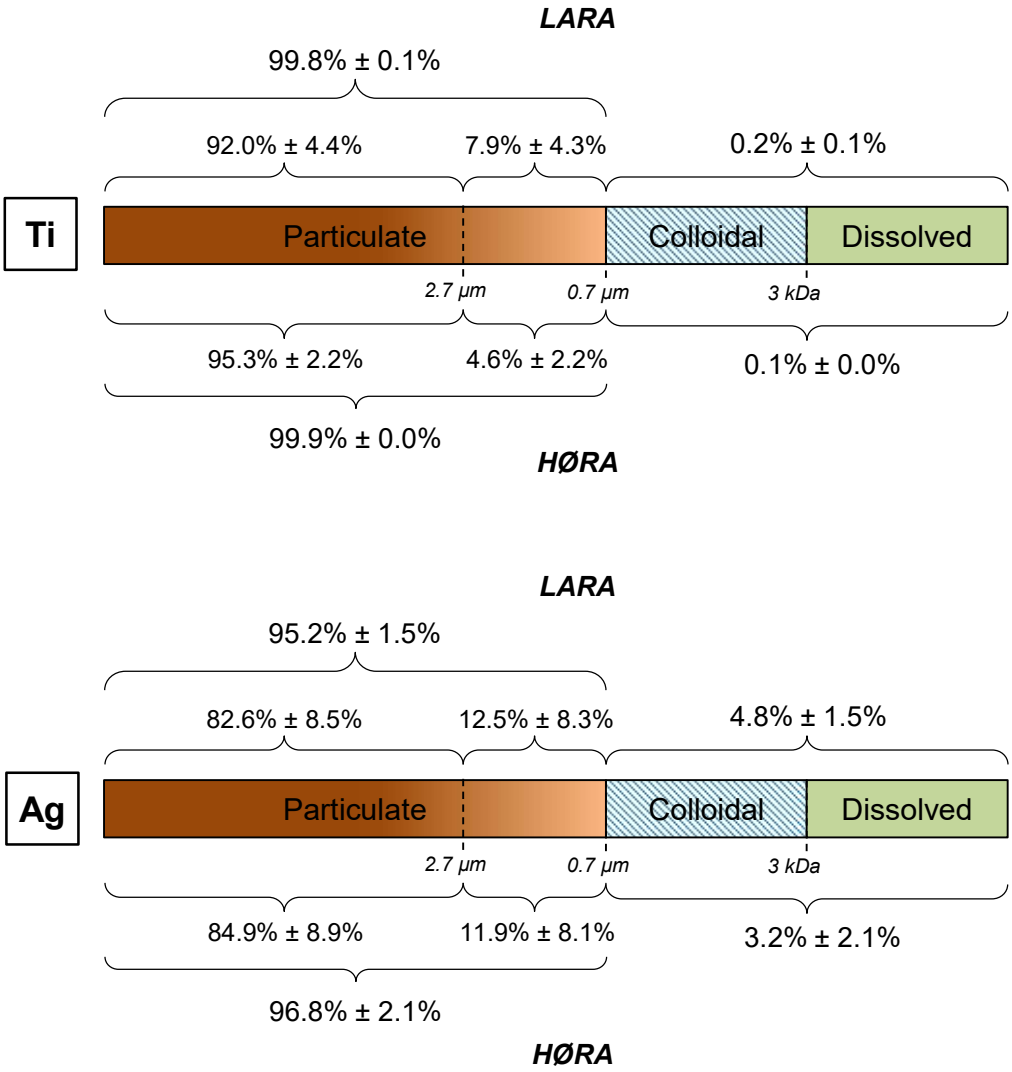

726

727 **Figure 5.** Fractionation of Ti and Ag in WWTP influents, and percentage composition of each
728 fraction (LARA: Ti: *n*=20, Ag: *n*=14; HØRA: Ti: *n*=18, Ag: *n*=14). For clarity, the bar lengths
729 of the individual fractions for Ti and Ag are not presented proportionally.

730

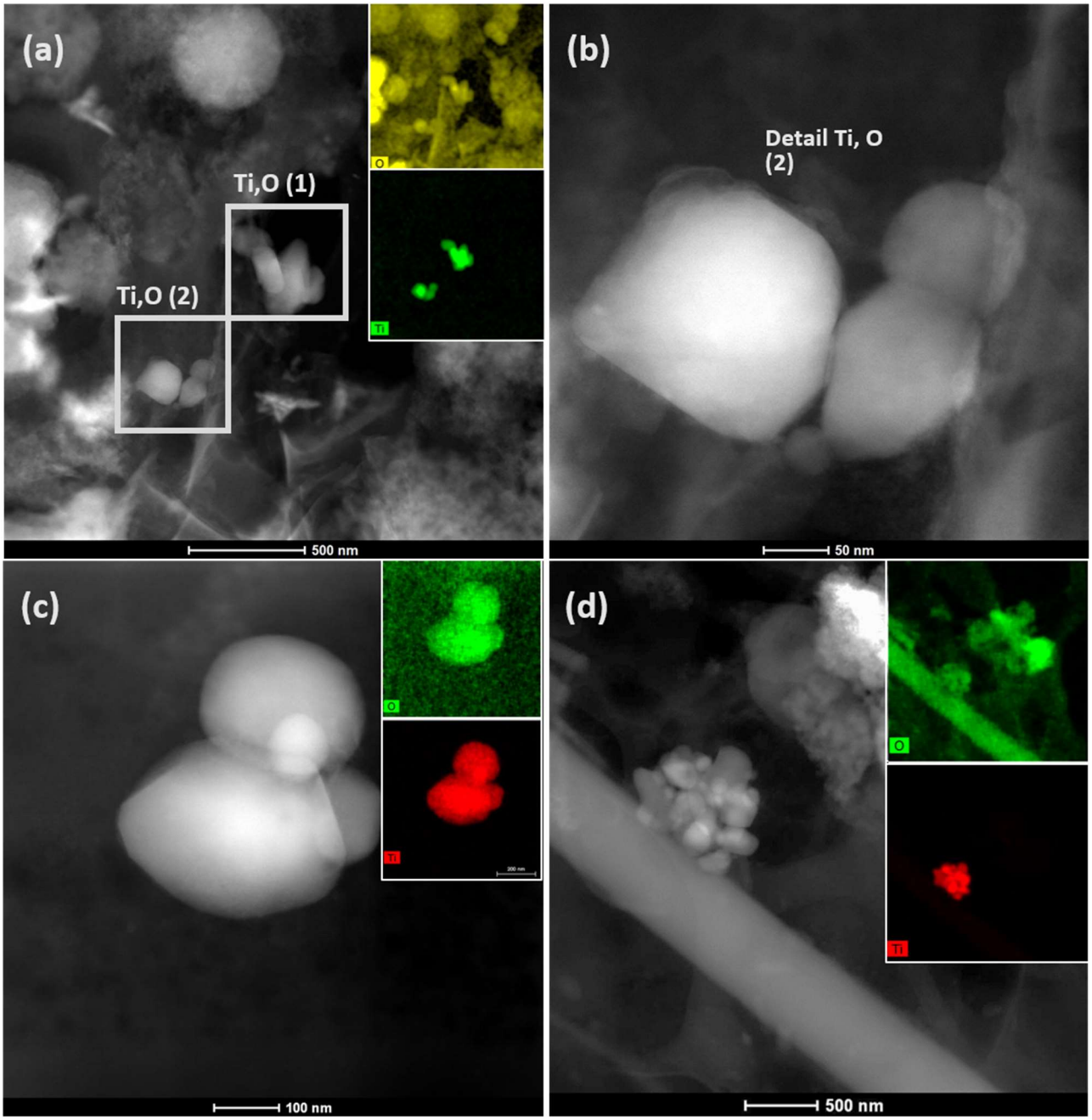

Figure 6. STEM images and elemental analysis (EDS, insert images) of TiO_2 particles in wastewater samples. (a) TiO_2 particles (O is displayed in yellow; Ti in green) in influent wastewater from LARA. Particles are associated with wastewater solids, with details shown in (b). Small (c) and large (d) agglomerates of TiO_2 particles (O shown in green, Ti in red) found in the particulate fraction (influent, evening sample E) from HØRA.

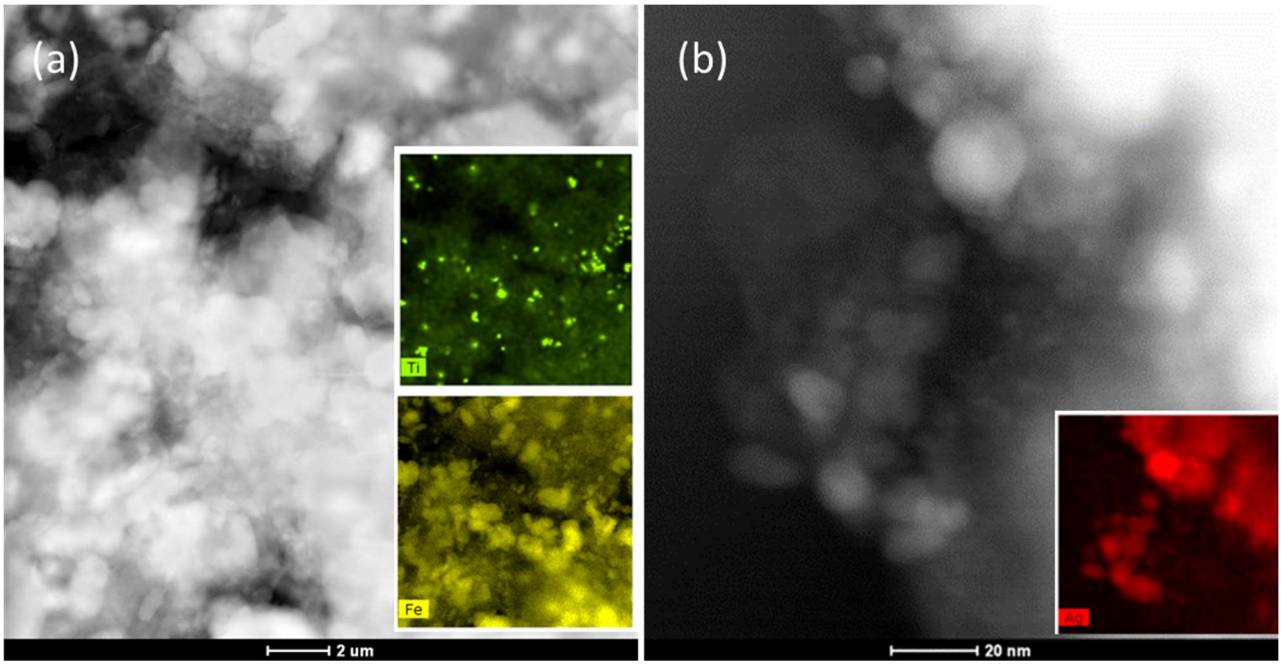

Figure 7. STEM images and elemental analysis (EDS; insert images) of biosolids samples (sludge) from LARA. (a) Ti particles (green) associated with Fe (yellow) containing material. (b) Ag NPs (Ag displayed in red).

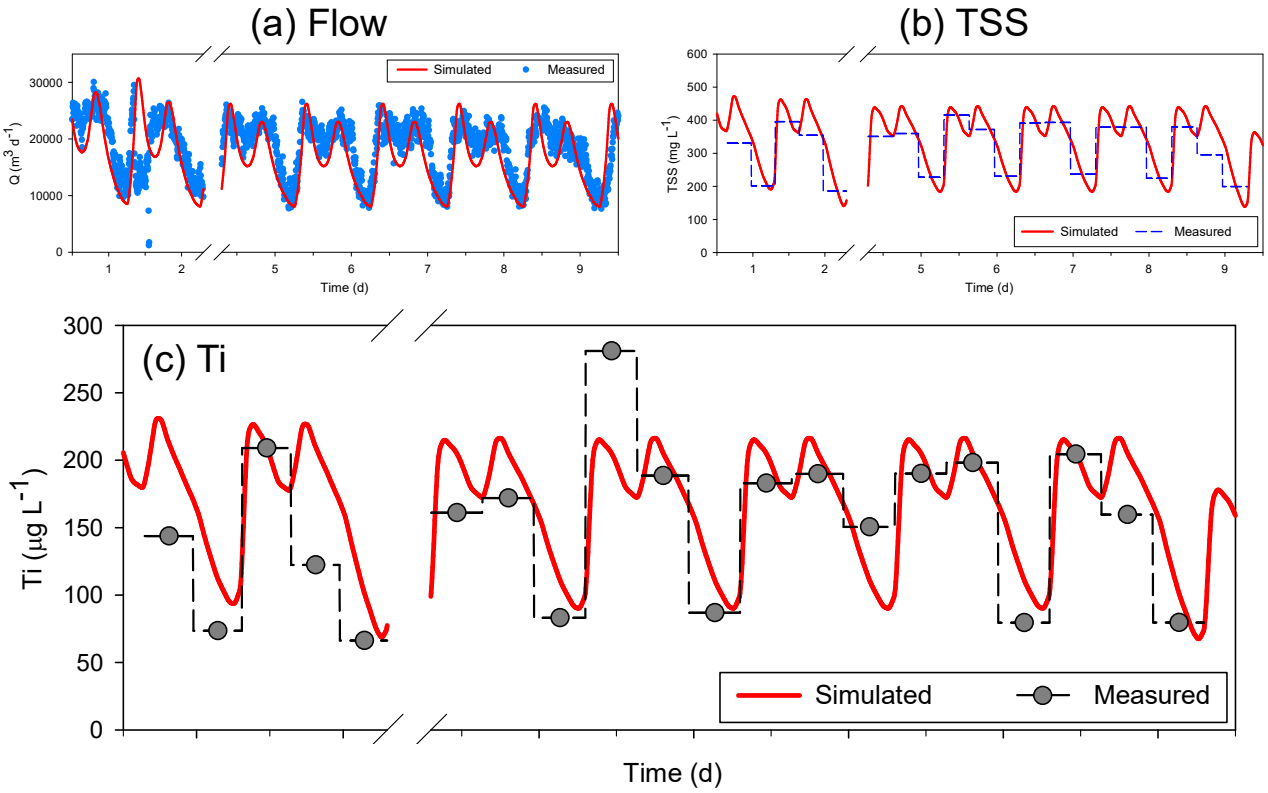

741

742 **Figure 8.** Measured and simulated profiles for (a) influent flow rate, (b) TSS concentration and

743 (c) Ti concentration in LARA during the sampling campaign period.

744

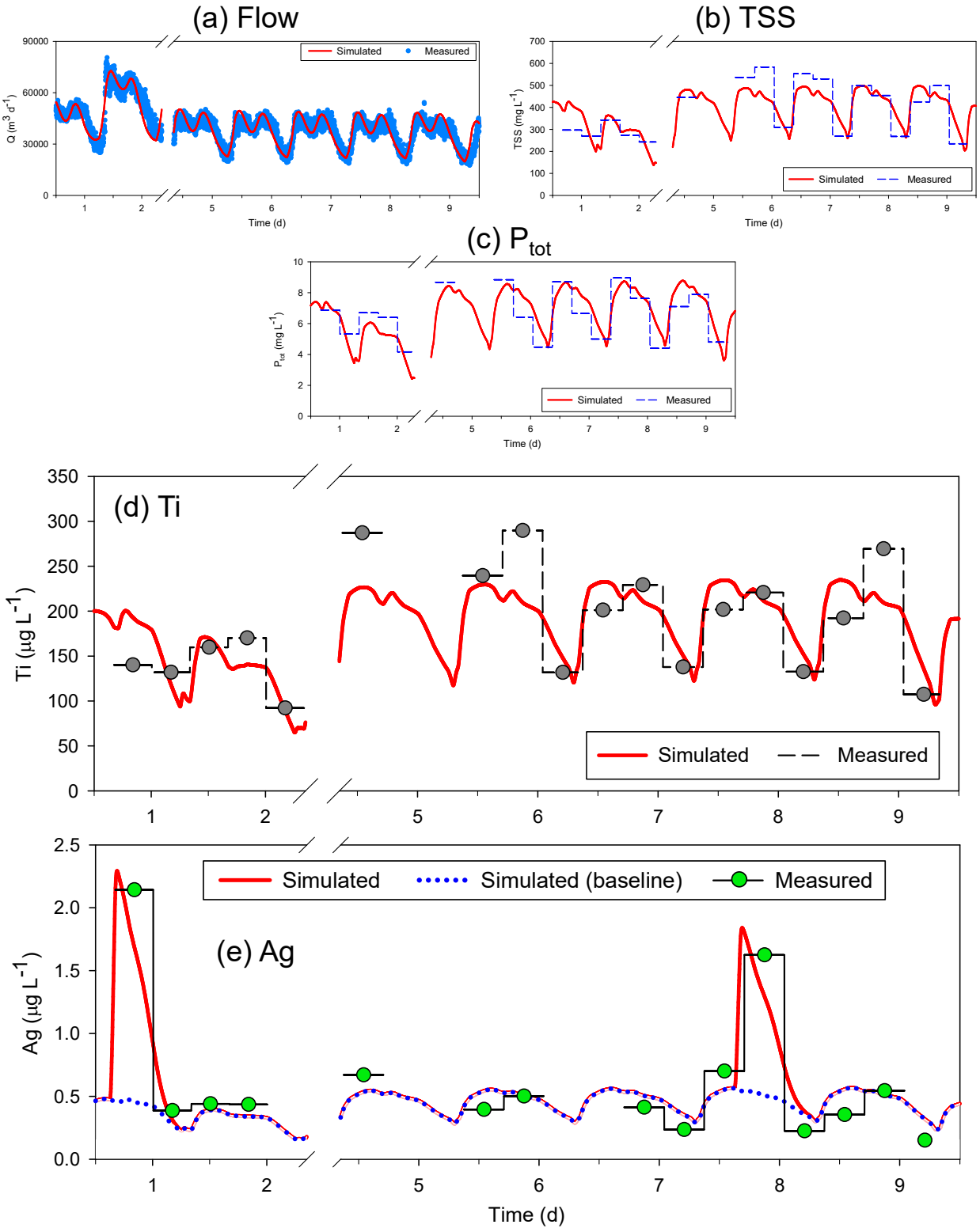

745

746 **Figure 9.** Measured and simulated profiles for (a) influent flow rate, (b–c) TSS and P_{tot}

747 concentrations, (d–e) Ti and Ag concentrations in HØRA during the sampling campaign.

748 Model simulations of peak Ag concentrations in influent (e) are shown in red.